JGR Solid Earth

RESEARCH ARTICLE
10.1029/2018JB017218

Modeling Ultralow Velocity Zones as a Thin Chemically Distinct Dense Layer at the Core-Mantle Boundary

John William Hernlund[1] and **Irene Bonati**[1]

[1]Earth-Life Science Institute, Tokyo Institute of Technology, Tokyo, Japan

Key Points:
- We derive an advection-diffusion equation that governs a chemically distinct ultralow-velocity zone at the base of a convecting mantle
- Solutions reveal compact structures with sharp lateral edges that accumulate beneath deep-rooted mantle upwellings
- A thin chemically distinct dense layer is predicted to be thin or absent in regions away from upwellings

Correspondence to:
J. W. Hernlund,
hernlund@gmail.com

Citation:
Hernlund, J. W., & Bonati, I. (2019). Modeling ultralow velocity zones as a thin chemically distinct dense layer at the core-mantle boundary. *Journal of Geophysical Research: Solid Earth*, *124*, 7902–7917. https://doi.org/10.1029/2018JB017218

Received 19 DEC 2018
Accepted 19 JUN 2019
Accepted article online 30 JUN 2019
Published online 14 AUG 2019

Abstract Seismically detected ultralow velocity zones (ULVZs) at the the core-mantle boundary reflect the dynamical state and geological evolution of the silicate-metal frontier of Earth's deep interior. However, modeling the dynamical context of ULVZs is hampered by challenges, such as the necessity of fine-scale resolution and the accurate treatment of large viscosity contrasts. Here we extend the treatment of ULVZs using a lubrication theory approach and apply it to numerical and analytical models relevant for mantle convection in the core-mantle boundary region. A generic model of a thin and dense low-viscosity ULVZ layer embedded between an overlying convecting viscous mantle and an underlying inviscid core can explain several features that are consistent with seismic inferences, such as the absence of ULVZs in some regions and a tabular shape where they are concentrated. The model explains how the topography of a ULVZ layer tends to saturate and flatten as it becomes thicker, due to a nonlinear feedback between viscous aggregation beneath upwelling mantle currents and gravitational spreading/relaxation. Implementation of the ULVZ equation in thermal convection models indicates that ULVZs are preferentially gathered beneath long-lived plumes and may not exist beneath newly formed plume roots where there is no source of layer material. The presence/absence of ULVZs and their detailed shapes may provide important insights into the dynamical state and convective instability of the lowermost mantle thermal boundary layer.

1. Introduction

Ultralow velocity zones (ULVZs) are small-scale (~10 km thick, ~100–1,000 km wide) regions at the core-mantle boundary (CMB; Garnero & Helmberger, 1996; Williams & Garnero, 1996) that are characterized by seismic velocity reductions of order ~10% and whose apparent stability and wide aspect ratios suggest higher densities relative to the overlying mantle (Garnero & McNamara, 2008; Hernlund & Tackley, 2007; Hernlund & McNamara, 2014). These tabular-like features may underlie some hot spots that are thought to be the surface manifestation of deep-seated upwelling hot mantle plumes (Cottaar & Romanowicz, 2012; Jellinek & Manga, 2002, 2004; Helmberger et al., 1998; Williams et al., 1998; Yuan & Romanowicz, 2017), and which exhibit a variety of chemical and isotopic anomalies (Jellinek & Manga, 2002). ULVZs are thought to be concentrated at regions of horizontally convergent flow above the CMB, such as plume roots at the borders of ~1,000-km scale chemically distinct large low shear velocity provinces (LLSVPs; Hernlund & Tackley, 2007; McNamara et al., 2010). ULVZs are also found in portions of the CMB region that are not associated with any candidate plume root or LLSVP boundary (Garnero et al., 2016; Li et al., 2017). Recently, somewhat larger "mega-ULVZ" structures have been reported in the Pacific region (Cottaar & Romanowicz, 2012; Jensen et al., 2013; Thorne et al., 2013). In terms of the magnitude of their seismic velocity variation, density contrast, thickness, and spatial variability, ULVZs are roughly analogous to the Earth's crust, although the geodynamical context differs in many respects.

Because of their pole position at the interface between Earth's lower mantle and outer liquid core, understanding the evolution of ULVZs is important for constraining the long-term thermal and chemical evolution of the CMB and the interactions (e.g., mass exchange) between Earth's mantle and core. However, the origin of ULVZs remains unclear and is a topic of active research (Hernlund & McNamara, 2014). The distinctiveness of these structures has been hypothesized to represent partially molten material as it circulates through the hot lower mantle thermal boundary layer (e.g., Rost et al., 2005; Williams & Garnero, 1996). However, the necessity for this kind of freshly generated partially molten mixture to attain a higher density (hence dynamically producing a wide aspect ratio), combined with inhibition of melt-solid separation to maintain its seismically anomalous character (Hernlund & Jellinek, 2010), implies a negative volume change upon melting that is not supported by mineral physics (Hernlund & Tackley, 2007). Another possibility is

that ULVZs represent chemically distinct material that has previously melted and accumulated at the CMB (Ohtani & Maeda, 2001) or was formed as the ancient fractionated residue of a more extensive basal magma ocean that prevailed in the hotter early Earth (Labrosse et al., 2007; Nomura et al., 2011; Wicks et al., 2010). Other ideas posit entrainment of metallic iron into silicates at the base of the mantle (Kanda & Stevenson, 2006; Petford et al., 2013). Present-day CMB structures, including ULVZs, might also reflect relics of the energetic accretion and segregation processes of the early solar system such as the Moon-forming giant impact, processes that may have contributed to the formation of deep mantle melts (Labrosse et al., 2015; Laneuville et al., 2018).

Whatever their origin may be, ULVZ shape and distribution may yield important clues about the nature of lowermost mantle dynamics, such as the planform of lowermost mantle convection, the existence of deep-seated plume roots or large-scale laterally distinct chemical domains, constraints on deep mantle rheology, the pattern of heat flux variations, and more. However, modeling of these structures presents some challenges. For example, incorporating the evolution of ULVZs in numerical models of large-scale mantle convection is computationally expensive due to their small spatial scale compared to the length scale of the mantle (∼0.1%). Past studies have investigated the dynamics and morphologies of chemically distinct dense ULVZ layers in 2-D by using a particle-based approach (McNamara et al., 2010), and more recently in 3-D for different ULVZ origin scenarios (Li et al., 2017). Compositionally distinct ULVZs have also been modeled using local boundary element formulations, revealing details of internal deformation behavior (Hier-Majumder & Drombosky, 2016). However, such methods remain computationally expensive, and it is possible that some details are not well resolved or may have other limitations. There may also be issues of numerical accuracy arising from tracer particle treatments for handling variations over length scales similar to the numerical discretization of the model. Finally, there are also limitations (both in extent and accuracy) with respect to resolving the large viscosity contrasts that might exist in ULVZs relative to the overlying mantle (Hier-Majumder & Revenaugh, 2010; Hernlund & Jellinek, 2010).

Here, we derive a simple way of mathematically modeling an ultrathin ULVZ layer at the bottom of the mantle by use of lubrication theory (Reynolds, 1886). The resulting "ULVZ equation" can be used to describe the evolution of ULVZs using either analytical or numerical tools (e.g., in mantle convection models). This approach is inspired by Hier-Majumder and Revenaugh (2010), who previously applied lubrication theory to arrive at approximate steady solutions for ULVZs with distinct chemical compositions residing beneath an axisymmetric upwelling flow (e.g., rooted beneath an upwelling hot mantle plume). They used these solutions, combined with seismological observations, to propose an estimate for the viscosity of ULVZs. Their results are consistent with viscosities of order $\sim 10^{18}$ Pa s, which could be considered relatively small for rocks in the lower mantle (Karato, 2014), although it is not clear a priori what kind of viscosity one should expect for ULVZ structures with potentially exotic chemical compositions. The present work is an expansion of this effort to include a more general derivation for time-dependent evolution and applications of the equation to a broader context.

The plan of this study is as follows: First, we derive the ULVZ equation by applying the thin-layer approximation to the Navier-Stokes equations relevant to this scenario. We then describe some basic analysis of the equation and explore the coupling between a thin dense layer and an overlying highly viscous mantle. We show how the areal coverage of ULVZs constrains the properties of the material that comprises it, which offers a unique observational approach for probing the properties of ULVZs. We then explore numerical solutions of the ULVZ equation as the main parameters are varied. Finally, we show how the ULVZ layer evolves in a simple 2-D thermal convection model and illustrate the ease with which a ULVZ layer can be included in any mantle convection code.

Using the time-dependent ULVZ equation, we arrive at several interesting results, which we examine in further detail later in the discussion. We show that chemically distinct ULVZs are swept into compact structures in time scales on the order of the residence time of mantle material circulating through the CMB region, leaving much of the top surface of the core exposed to mantle material circulating into the CMB region from above. We also show that the fractional coverage of ULVZs over the CMB constrains intrinsic ULVZ properties such as density and viscosity if the form of mantle circulation is known. Testing the ULVZ equation in mantle convection models at high convective vigor shows that compositionally distinct ULVZs reside at the root of old plumes and may not be present beneath newly formed plumes, offering a possible independent test of the degree of convective instability of the lowermost mantle thermal boundary layer. A slight

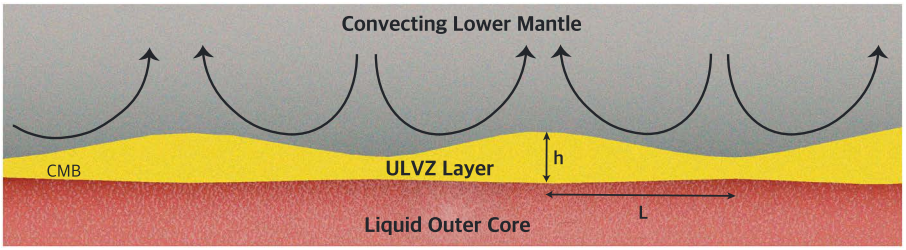

Figure 1. Schematic representation of a chemically distinct ULVZ layer subject to deformation by mantle flow. The h ~10-km-thin ULVZ layer (yellow) overlies the liquid outer core (red) and varies over lateral length scales L ~100 km. ULVZ = ultralow velocity zone; CMB = core-mantle boundary.

asymmetry in the shape of ULVZs is produced by lateral motion of plumes along the CMB, with thickening in the direction of plume migration, and such features might be used to investigate the dynamical state of the lowermost mantle.

2. Derivation of the ULVZ Equation

Here we describe the derivation of the equation governing the evolution of a thin chemically distinct layer at the CMB. The approach is closely related to the lubrication theory developed by Reynolds (1886), which is a special case in fluid dynamics that deals with the scenario in which a fluid layer of thickness h exhibits variations over perpendicular length scales L that are comparatively much larger in magnitude than h. Here we consider variations in h to be of order h (consistent with our later findings). When one assumes $h/L \ll 1$, called the "thin-layer approximation," the equations governing fluid flow in the layer can be simplified dramatically. In the following, we derive an equation governing a thin layer with positive anomalous density $\Delta\rho$ (relative to the mantle) embedded beneath a creeping highly viscous half-space (i.e., the convecting rocky solid mantle) and resting upon a denser inviscid substrate (i.e., the liquid outer core). The basic context of the ULVZ layer is shown in Figure 1.

For simplicity, in this development we adopt a Cartesian reference frame with orthonormal coordinates x, y, and z (where z varies in the vertical direction) and time denoted by t. The thickness of the ULVZ is negligible in comparison with the curvature (i.e., 1/radius) of the CMB. It is straightforward to extend the results to other coordinate systems, so long as any assumptions made in one coordinate system (e.g., the direction of gravity) remain valid in the new one. Our thin layer is confined between the plane at $z = 0$ (CMB) and the surface $z = h(x, y) > 0$. Although a perfectly flat bottom boundary is not strictly valid for a dense ULVZ layer, which is expected to protrude slightly into the underlying core as it thickens (Hernlund & Tackley, 2007), the assumption of bottom flatness will not influence the resulting governing equation.

2.1. Transport Equation

We first describe the motion of the layer surface at $z = h$ (i.e., the top of the ULVZ) in terms of the fluid velocities at the top the layer, with v_x, v_y, and v_z being the x-, y-, and z components of the velocity at $z = h$. We define a "level set" function $f(x, y, z, t) = z - h(x, y, t)$, such that $f = 0$ at the interface between the layer and overlying material. The surface moves from any position x, y, and z at time t to a position $x + v_x\delta t, y + v_y\delta t, z + v_z\delta t$ at time $t + \delta t$. Expanding f as a Taylor series in δt gives

$$f(x + v_x\delta t, y + v_y\delta t, z + v_z\delta t, t + \delta t) = f(x, y, z, t) + \left(\frac{\partial f}{\partial t} + \vec{v}\cdot\vec{\nabla}f\right)\delta t + O(\delta t^2). \quad (1)$$

Because $f(x, y, z, t) = 0$ at all times, both the left side and the first term on the right side of equation (1) vanish. Taking the limit $\delta t \to 0$ then gives the following result:

$$\frac{\partial f}{\partial t} + \vec{v}\cdot\vec{\nabla}f = 0. \quad (2)$$

For convenience of notation, we use a subscript H to denote a vector with only horizontal components (i.e., no z component) and denote $v_z(x, y, z = h, t) = V(x, y, t)$ and $\vec{v}_H(x, y, z = h, t) = \vec{U}(x, y, t)$. Equation (2) can then be rewritten in the following form:

$$\frac{\partial f}{\partial t} + V\frac{\partial f}{\partial z} + \vec{U}\cdot\vec{\nabla}_H f = 0. \quad (3)$$

Substituting $f = z - h$, a transport equation governing h in terms of V and $\vec{U}$ is obtained:

$$\frac{\partial h}{\partial t} = V - \vec{U} \cdot \vec{\nabla}_{\mathrm{H}} h. \tag{4}$$

2.2. Conservation of Mass

Fluid flow in the thin layer is well approximated as incompressible, in which case the conservation of mass inside the layer is given by

$$\frac{\partial v_{\mathrm{z}}}{\partial z} + \vec{\nabla}_{\mathrm{H}} \cdot \vec{v}_{\mathrm{H}} = 0. \tag{5}$$

2.3. Conservation of Momentum

If we assume that gravity is antiparallel to the z-axis and neglect the influence of fluid inertia, the equation governing conservation of momentum in the vertical direction can be written as

$$\mu \nabla_{\mathrm{H}}^2 v_{\mathrm{z}} + \mu \frac{\partial^2 v_{\mathrm{z}}}{\partial z^2} - \frac{\partial p}{\partial z} - \Delta\rho g = 0, \tag{6}$$

and in the horizontal direction(s)

$$\mu \nabla_{\mathrm{H}}^2 \vec{v}_{\mathrm{H}} + \mu \frac{\partial^2 \vec{v}_{\mathrm{H}}}{\partial z^2} - \vec{\nabla}_{\mathrm{H}} p = 0, \tag{7}$$

where p is the nonhydrostatic (dynamic) pressure variation, $\Delta\rho$ is the positive density anomaly of the thin layer, μ is its dynamic viscosity, and $\nabla_{\mathrm{H}}^2 = \vec{\nabla}_{\mathrm{H}} \cdot \vec{\nabla}_{\mathrm{H}}$.

2.4. Thin-Layer Approximation

The relative magnitude of terms in the governing equations (4)–(7) for a thin layer can be assessed by replacing $\vec{\nabla}_{\mathrm{H}} \sim 1/L$ and $\partial/\partial z \sim 1/h$, where the symbol "~" is meant to convey "is on the order of." Performing this substitution in equations (5)–(7) results in

$$\frac{\delta V}{h} + \frac{\delta U}{L} \sim 0, \tag{8}$$

$$\mu \delta V \left(\frac{h}{L}\right)^2 + \mu \delta V + \delta p h + \Delta\rho g h^2 \sim 0, \tag{9}$$

and

$$\mu \delta U \left(\frac{h}{L}\right)^2 + \mu \delta U + \frac{\delta p h^2}{L} \sim 0, \tag{10}$$

where δV, δU, and δp denote the corresponding magnitudes of velocity and pressure variations. The first terms in (9)–(10) vary like $(h/L)^2$, and we anticipate that they become negligibly small in the limit $h/L \to 0$. In such a case the residual terms in equation (10) reduce to

$$\mu \delta U \sim \frac{\delta p h^2}{L}. \tag{11}$$

Using both equations (8) and (11), the residual terms for equation (9) then reduce to

$$\mu \delta V + \delta p h + \Delta\rho g h^2 \sim \left(\frac{h}{L}\right)^2 \delta p h + \delta p h + \Delta\rho g h^2 \sim 0, \tag{12}$$

showing that the term representing the relative contribution of $\mu \partial^2 v_{\mathrm{z}}/\partial z^2$ is also of order $(h/L)^2$. Therefore, in the limit $h/L \to 0$ we expect that $\mu \partial^2 v_{\mathrm{z}}/\partial z^2 \to 0$, which implies that variations in v_{z} of order higher than linear in z may be neglected in a thin-layer context. After eliminating all terms of order $(h/L)^2$ the simplified momentum equations may be written as

$$\frac{\partial p}{\partial z} \approx -\Delta\rho g \tag{13}$$

and

$$\mu \frac{\partial^2 \vec{v}_{\mathrm{H}}}{\partial z^2} \approx \vec{\nabla}_{\mathrm{H}} p. \tag{14}$$

2.5. Integrated Thin-Layer Equation

For boundary conditions appropriate to ULVZs, the upper surface at $z = h$ is in contact with the overlying mantle and has the same velocity $(V, \vec{U})$ and dynamic pressure (p) at the interface. The lower surface of the layer at $z = 0$ is considered to be impenetrable (i.e., $v_z = 0$) and shear stress free (i.e., $\partial \vec{v}_H / \partial z = 0$). We assume that $L \gg h$ and the thin-layer limit applies, such that the approximation can be expressed as an equality. Integrating equation (13) from $z = 0$ to $z = h$:

$$\int_0^h \frac{\partial p}{\partial z} dz = p(x, y, h) - p(x, y, 0) = \Pi - p(x, y, 0) = -\Delta \rho g h, \tag{15}$$

where $\Pi(x, y) = p(x, y, h)$ is the dynamic (i.e., departure from hydrostatic) pressure at the top of the layer (equal to the dynamic pressure at the base of the overlying mantle) and $p(x, y, 0)$ is the pressure at the bottom of the layer. Substituting equation (15) into equation (14),

$$\mu \frac{\partial^2 \vec{v}_H}{\partial z^2} = \vec{\nabla}_H (\Delta \rho g h + \Pi), \tag{16}$$

and twice integrating over the layer in z while applying the boundary conditions,

$$\vec{v}_H = \vec{U} + \left(z^2 - h^2\right) \frac{1}{2\mu} \vec{\nabla}_H (\Delta \rho g h + \Pi). \tag{17}$$

Integrating the mass conservation equation (5) in z gives

$$\int_0^h \left(\frac{\partial v_z}{\partial z} + \vec{\nabla}_H \cdot \vec{v}_H \right) dz = V - \vec{U} \cdot \vec{\nabla}_H h + \vec{\nabla}_H \cdot \left(\int_0^h \vec{v}_H dz \right) = 0. \tag{18}$$

Combining equations (4), (17), and (18), the result is

$$\frac{\partial h}{\partial t} + \vec{\nabla}_H \cdot \left(\vec{U} h \right) = \vec{\nabla}_H \cdot \left[\frac{h^3}{3\mu} \vec{\nabla}_H (\Delta \rho g h + \Pi) \right]. \tag{19}$$

Equation (19) assumes the form of an advection-diffusion equation governing variations of h. This result is the same as equation 12 in Hier-Majumder and Revenaugh (2010), except that their expression was written specifically for axisymmetric geometry at steady state conditions and additionally neglected lateral variations in dynamic pressure Π at the top of the layer.

3. Basic Analysis of the ULVZ Equation

3.1. Importance of Mantle Dynamic Pressure Variations

Large-scale flow in the overlying mantle is governed by momentum equations similar to equations (6) and (7). The horizontal length scale L that controls the lateral movements of the ULVZ layer is a scale that should be characteristic of larger-scale mantle convection patterns. The vertical length scale of mantle convection H is typically expected to be much larger than the thickness of the ULVZ layer (i.e., $H \gg h$). Substituting these length scales for the spatial derivatives in equations (6) and (7), we have

$$\mu_m \left(\frac{1}{H^2} + \frac{1}{L^2} \right) \delta v_z + \frac{\delta \Pi}{H} + \delta \rho_m g \sim 0, \tag{20}$$

$$\mu_m \left(\frac{1}{H^2} + \frac{1}{L^2} \right) \delta v_H + \frac{\delta \Pi}{L} \sim 0, \tag{21}$$

where $\delta \rho_m$ is the magnitude of density fluctuations that drive mantle convection through the buoyancy force (~1%), μ_m is the overlying mantle viscosity, and $\delta \Pi$ is the dynamic pressure variations associated with mantle convection. Using $\delta v_H / \delta v_z \sim L/H$ from conservation of mass and combining equations (20) and (21),

$$\delta \Pi \sim \delta \rho_m g L \frac{(H/L)^2}{1 + (H/L)}. \tag{22}$$

Mantle dynamic pressures should be compared with the magnitude of pressure changes associated with variations in the thickness of the ULVZ layer (i.e., $\Delta \rho g h$),

$$\frac{\delta \Pi}{\Delta \rho g h} \sim \left(\frac{\delta \rho_m}{\Delta \rho} \right) \left(\frac{L}{h} \right) \frac{(H/L)^2}{1 + (H/L)}. \tag{23}$$

While it is possible that $\delta\rho_m/\Delta\rho \sim 10^{-1}$ if ULVZ are ~10% more dense than overlying mantle, the ratio L/h should be large (by 1 or more orders of magnitude) consistent with the assumptions of the thin-layer approximation. If $H \sim L$ for the largest scales of mantle convection, then we are forced to conclude that Π is not necessarily small in comparison to $\Delta\rho g h$, and therefore, it cannot be safely neglected on the right-hand side of equation (19). We will accordingly retain pressure variations in the model and examine their role in more detail in a later section.

3.2. Deformation of the Overlying Mantle by Thinning/Thickening of ULVZs

When the ULVZ layer migrates laterally in a uniform mantle flow, then there is no dynamic coupling between the ULVZ internal deformation and the overlying mantle. Instead, the layer is passively swept along in the mantle "wind." However, when the ULVZ thins (or thickens) by processes related to gravitational relaxation, it is coupled to viscous deformation of the overlying mantle that may exert an additional resisting force, and this kind of coupling was not considered in the derivation of the thin-layer approximation above. Because the mantle may be highly viscous in comparison to ULVZs, neglect of mantle stresses in treating ULVZ topographic diffusion could potentially lead to inaccuracies and undermine the validity of the thin-layer approximation. The present situation differs from some common applications of Reynolds' lubrication theory, such as fluid layers embedded between rigid boundaries (hence fixing h) or fluid layers situated beneath an inviscid half-space. We therefore assess whether this special case raises any difficulties in applying the ULVZ equation.

Consider a portion of an existing ULVZ layer of horizontal scale L_t, which is slightly thicker by an amount δh_t relative to surrounding ULVZ material that has a thickness $h = h_0$. In the absence of indirect influences by mantle convection, the layer will undergo viscous relaxation analogous to diffusion until it has a uniform thickness, and the anomalously high interface will depress vertically by an amount $\sim \delta h_t$. The diffusion time for relaxation is $\sim 3\mu L_t^2/(\Delta\rho g h_0^3)$ so that the rate of change in ULVZ topography will be of order $\delta v_{zt} \approx \delta h_t \Delta\rho g h_0^3/(3\mu L_t^2)$. The mantle overlying the elevated ULVZ sinks at the same rate δv_{zt}. The viscous stress associated with corresponding deformation of the overlying mantle is then $\tau_t \sim \mu_m \delta v_{zt}/L_t \sim \delta h_t \mu_m \Delta\rho g h_0^3/(3\mu L_t^3)$. If the induced mantle stress is to be neglected in comparison to thin-layer dynamics taken in isolation, then we should expect that it is smaller in order of magnitude (i.e., ~10 times) than the pressure effect associated with the topographic relaxation, $\Delta\rho g \delta h_t$, which implies that the following condition should be met:

$$\frac{h_0}{L_t} \lesssim \left(\frac{\mu}{10\mu_m}\right)^{1/3}. \tag{24}$$

From this expression we note that the validity of using the ULVZ equation alone (i.e., without explicit coupling to overlying mantle flow) depends on the viscosity ratio between the overlying mantle and the ULVZ layer itself. In particular, the extent to which h must be smaller than L becomes more strict as the ULVZ layer becomes less viscous in comparison to the overlying mantle.

In order to assess the validity of neglecting deformation of the overlying mantle, consider a ~10-km-thick ULVZ relative to mantle convection length scales of ~1,000 km. In such a case, the limit in equation (24) is satisfied for viscosity contrasts as large as $\mu_m/\mu \sim 10^5$, which extends well beyond previous estimates for ULVZs (e.g., Hier-Majumder & Revenaugh, 2010). Care should be taken, however, in extending the thin-layer approximation to more extreme viscosity ratios.

3.3. Expression in Terms of Basal Strain Rate

The manner in which mantle flow varies near the CMB and couples to a thin ULVZ layer can be simplified using similar arguments as those involved in the thin-layer approximation. The vertical velocity variation in z can be expanded as a Taylor series:

$$v_z(z) = v_z(z=0) + z\left(\frac{\partial v_z}{\partial z}\right)_{z=0} + \frac{z^2}{2}\left(\frac{\partial^2 v_z}{\partial z^2}\right)_{z=0} + \ldots = z\left(\frac{\partial v_z}{\partial z}\right)_{z=0} + \frac{z^2}{2}\left(\frac{\partial^2 v_z}{\partial z^2}\right)_{z=0} + \ldots. \tag{25}$$

The previous development leading to equation (12) demonstrated that $\partial^2 v_z/\partial z^2 \sim h/L$ in the context of a thin layer, and it follows that $\partial^3 v_z/\partial z^3$ and higher derivatives vary with higher order in h/L (which are assumed to be negligible in the thin-layer approximation). At $z = h$ we have

$$V = -h\dot{\varepsilon} + \frac{h^2}{2}\left(\frac{\partial^2 v_z}{\partial z^2}\right)_{z=0} + \ldots \sim h + h^2\frac{h}{L} + \ldots, \tag{26}$$

where we define the characteristic pure shear strain rate:

$$\dot{\varepsilon} = -(\partial v_z/\partial z)_{z=0}. \tag{27}$$

Taking the horizontal divergence ($\vec{\nabla}_H \cdot$) of the horizontal momentum equation (7) and applying $h \ll L$ results in

$$\mu_m \nabla_H^2 \left(\vec{\nabla}_H \cdot \vec{v}_H\right) + \mu_m \frac{\partial^2}{\partial z^2}\left(\vec{\nabla}_H \cdot \vec{v}_H\right) - \nabla_H^2 p = \nabla_H^2\left(\mu_m \dot{\varepsilon} - p\right) - \mu_m \frac{\partial^3 v_z}{\partial z^3} \approx \nabla_H^2\left(\mu_m \dot{\varepsilon} - p\right) = 0. \tag{28}$$

This development uses $\vec{\nabla}_H \cdot \vec{v}_H = -\dot{\varepsilon}$ via equation (5).

The solution to equation (28) is

$$p = \mu_m \dot{\varepsilon} + \psi, \tag{29}$$

where ψ is any function that satisfies $\nabla_H^2 \psi = 0$. In a horizontally periodic domain such as the mantle, the only solution is $\psi =$ constant, which we can take to be zero since this term is acted upon by the gradient operator. Therefore, we set $\Pi = \mu_m \dot{\varepsilon}$, in which case the equation governing variations in a chemically distinct ULVZ layer becomes

$$\frac{\partial h}{\partial t} + \vec{\nabla}_H \cdot \left(\vec{U} h\right) = \vec{\nabla}_H \cdot \left[\frac{h^3}{3\mu} \vec{\nabla}_H (\Delta \rho g h + \mu_m \dot{\varepsilon})\right]. \tag{30}$$

Note that this equation contains two different viscosities, μ and μ_m, representing values appropriate for the ULVZ and the overlying mantle, respectively.

3.4. Basic Aspects of the ULVZ Equation

The dynamical behavior of a thin layer and its relationship to overlying mantle flow is relatively straightforward to describe using the equations developed above. Equation (30) can be expanded to give

$$\frac{Dh}{Dt} = \frac{\partial h}{\partial t} + \vec{U} \cdot \vec{\nabla} h = -\dot{\varepsilon} h + \vec{\nabla}_H \cdot \left(\frac{\Delta \rho g h^3}{3\mu} \vec{\nabla}_H h\right) + \vec{\nabla}_H \cdot \left(\frac{\mu_m h^3}{3\mu} \vec{\nabla}_H \dot{\varepsilon}\right), \tag{31}$$

where D/Dt denotes the time derivative in a Lagrangian frame of reference moving with velocity $\vec{U}$. The first term on the right-hand side of equation (31) represents thinning or thickening of the layer driven by flow divergence or convergence, respectively. For a spatially uniform h and constant $\dot{\varepsilon}$ the solution for layer evolution dictated by this remaining term is simply

$$h = h(t = t_0) \exp\left[-\dot{\varepsilon}(t - t_0)\right]. \tag{32}$$

The influence of horizontally divergent or convergent flow is to thin or thicken the layer with an e-fold time scale of $1/\dot{\varepsilon}$.

The second diffusion-like term on the right side of equation (31) represents the viscous relaxation of variations in layer thickness. The effective diffusivity of topography variation is apparently

$$D = \frac{\Delta \rho g h^3}{3\mu}, \tag{33}$$

which is sensitive to layer thickness. Note that the diffusivity of topography is small for small h but becomes rapidly stronger (varying as h^3) when h grows in magnitude. This behavior will later be seen to saturate/flatten ULVZ topography as the layer thickens, since variations in topography diffuse more rapidly where the layer is thick.

The third term on the right side of equation (31) reflects the action of dynamic pressure variations imposed from above by large-scale flows. These pressure variations can also drive flows within the ULVZ layer, resulting in changes in the layer thickness.

3.5. Nondimensionalization

Consider a layer of average global thickness h_0, to which the layer would eventually decay in the absence of viscous coupling to mantle deformation. Assuming a reference length scale L, time scale τ, and denoting nondimensionalized quantities with a prime, we can rewrite equation (19) as

$$\frac{\partial h'}{\partial t'} + \vec{\nabla}'_{\mathrm{H}} \cdot \left(\vec{U}' h'\right) = \vec{\nabla}'_{\mathrm{H}} \cdot \left[D_{\mathrm{u}} h'^3 \vec{\nabla}'_{\mathrm{H}} (h' + \Pi')\right], \tag{34}$$

where

$$h' = \frac{h}{h_0}, \tag{35}$$

$$t' = \frac{t}{\tau}, \tag{36}$$

$$\vec{\nabla}'_{\mathrm{H}} = L\vec{\nabla}_{\mathrm{H}}, \tag{37}$$

$$\vec{U}' = \vec{U}\frac{\tau}{L}, \tag{38}$$

$$\Pi' = \frac{\Pi}{\Delta\rho g h_0} = \frac{\mu_{\mathrm{m}}\dot{\varepsilon}}{\Delta\rho g h_0}, \tag{39}$$

and there is a nondimensional parameter that scales the diffusivity of topography variations:

$$D_{\mathrm{u}} = \frac{\Delta\rho g h_0^3 \tau}{3\mu L^2}. \tag{40}$$

Assuming estimates of $\Delta\rho \approx 500$ kg/m^3 (i.e., 10%), $g \approx 10$ m/s^2, $\tau \approx 10$ Myrs, $L \approx 5{,}000$ km, $\mu \approx 10^{18}$–10^{21} Pa s, and $h_0 \approx 100$–$1{,}000$ m, the parameter D_{u} would assume values in the range $D_{\mathrm{u}} = 10^{-11}$–$10^{-5}$. The large (6 orders of magnitude) uncertainty in D_{u} is exacerbated by the unknown average thickness h_0 and poorly constrained ULVZ viscosity μ. Appropriate choice of length and time scales also exerts an important influence and carries uncertainties that need to be better constrained by other considerations.

In mantle convection models one typically nondimensionalizes the governing equations using a mantle thickness L_{m} and thermal diffusion time scale of L_{m}^2/κ, in which case we have

$$D_{\mathrm{u}} = \frac{\Delta\rho g h_0^3}{3\mu\kappa}, \tag{41}$$

which is independent of the mantle length scale L_{m}. Pressure in mantle convection models that use L_{m} and L_{m}^2/κ as spatial and temporal measures are nondimensionalized by the factor $\mu_{\mathrm{m}}\kappa/L_{\mathrm{m}}^2$, so that

$$\Pi' = \frac{\Pi}{\Delta\rho g h_0} = p'_{\mathrm{m}} \frac{\mu_{\mathrm{m}}\kappa}{\Delta\rho g h_0 L_{\mathrm{m}}^2} = \frac{p'_{\mathrm{m}}}{Ra} \frac{\rho_0 \alpha \Delta T L_{\mathrm{m}}}{\Delta\rho h_0} = \frac{p'_{\mathrm{m}}}{Ra} \frac{\Delta\rho_{\mathrm{T}} L_{\mathrm{m}}}{\Delta\rho h_0}, \tag{42}$$

where p'_{m} is the nondimensional deviatoric mantle convection pressure, ρ_0 is a reference density, α is the thermal expansivity, ΔT is the super-adiabatic temperature change, and

$$Ra = \frac{\rho_0 g \alpha \Delta T L_{\mathrm{m}}^3}{\mu_{\mathrm{m}}\kappa} \tag{43}$$

is the Rayleigh number. The quantity $\Delta\rho_{\mathrm{T}}$ is the thermal density change that drives purely thermal mantle convection.

3.6. Advection Versus Diffusion and Steady State Relations

Advection-diffusion-type problems are sometimes characterized by comparing the magnitude of the advection term relative to the diffusion term, leading to a nondimensional "Peclet number" (*Pe*). In the context of mantle convection, *Pe* usually refers to the advection of heat relative to thermal diffusion:

$$Pe_T = \frac{U\nabla T}{\kappa\nabla^2 T} \sim \frac{\bar{U}L}{\kappa}, \tag{44}$$

where $\bar{U}$ is the characteristic advective velocity for transport and κ is the thermal diffusivity. In the present case of ULVZ advection-diffusion, we could define an analogous Peclet number:

$$Pe_U = \frac{U\nabla h}{D\nabla^2 h} \sim \frac{\bar{U}L}{D} = \frac{3\mu\bar{U}L}{\Delta\rho g h^3}. \tag{45}$$

If a steady state solution to an advection-diffusion equation exists for a particular scenario, then it follows that $Pe \rightarrow \sim 1$ as $t \rightarrow \infty$. In linear problems the solution trends toward $Pe \sim 1$ for a given velocity field by adopting a steady length scale L_S. A typical example (e.g., Hernlund, 2010) is a steady thermal boundary layer of thickness $L_S \sim \kappa/\bar{U}$. In the ULVZ equation the nonlinearity of diffusivity offers an additional degree of freedom, and at steady state we expect

$$\frac{h^3}{L} \rightarrow \frac{h_u^3}{L_u} \sim \frac{3\mu\bar{U}}{\Delta\rho g}, \tag{46}$$

which permits both h and L to evolve to the values h_u and L_u that balance advection and diffusion. This relationship will be used later in analyzing our numerical modeling results for the steady state shape of ULVZs.

4. Numerical Solutions of the ULVZ Equation

In this section we explore time-dependent solutions of the ULVZ equation in order to understand the basic behavior of a compositionally distinct dense layer embedded at the CMB. We first examine the case of an imposed steady mantle flow and consider the time evolution of an initially uniform ULVZ layer to steady state. We then turn our attention to ULVZ evolution in a time-dependent mantle flow for mantle convection at relatively high Rayleigh number.

4.1. Notes on the Numerical Treatment of the ULVZ Equation

The ULVZ equation (34) is an advection-diffusion equation that can be integrated using standard numerical techniques, although we have found that special care should be taken in treating the nonlinear diffusivity term. In the following examples we employ finite volume flux-limited advection and implicit diffusion, while pressure is treated as a source term. The advection, diffusion, and source term evolutions are treated independently. For the diffusivity, we use values of h' from the previous time step to obtain an estimate of the solution at the next time step. We have found that implicit time integration is needed for diffusion owing to the large variations in diffusivity ($d = D_u h'^3$) that typically arise and evolve with the solution. In our finite volume scheme, the diffusivity needs to be interpolated from locations where h' is naturally defined (e.g., cell centers) to intermediate points (i.e., cell vertices). Care must be taken in this step when sharp edges of ULVZ structures arise as part of the solution. We use a harmonic interpolation of the diffusivity $2d_1d_2/(d_1 + d_2)$ between adjacent values d_1 and d_2 when $|\log(d_1/d_2)| < 1$ and linear interpolation $(d_1 + d_2)/2$ when $|\log(h_1/h_2)| \geq 1$.

4.2. Evolution of a ULVZ Layer in an Imposed Mantle Flow

We first examine numerical solutions for a thin layer situated between a downwelling and upwelling center in the deep mantle. We assume a particular form for the flow velocity in the mantle (Figure 2) and solve the ULVZ equation for the evolution of the layer. This affords an opportunity to examine the characteristics of the solution in detail. We consider two geometries: a 2-D Cartesian case where the upwelling and downwelling flow on either side of the domain is sheetlike, and an axisymmetric case in which a cylindrical upwelling is situated at the axis of a convergent flow at the CMB. In these models we choose the horizontal distance between downwelling and upwelling centers L_r as a length scale and the residence time $\tau_r = L_r/U_0$ as a time scale, where U_0 is the characteristic horizontal flow velocity at the CMB. Under these conditions the

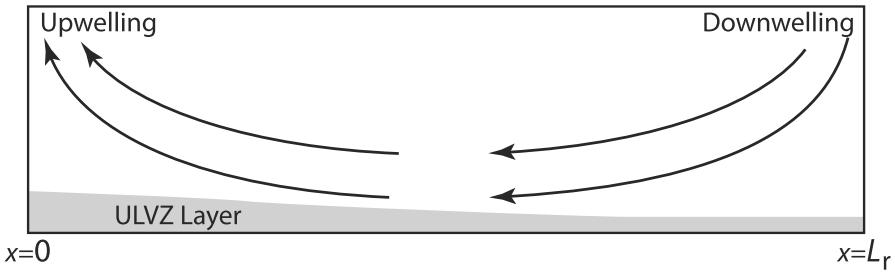

Figure 2. Schematic illustration of the context for the evolution of a ULVZ layer in an imposed mantle flow.

parameters are defined as

$$D_{\mathrm{u,res}} = \frac{\Delta\rho h_0^3}{3\mu U_0 L_\mathrm{r}} \tag{47}$$

and

$$\Pi' = \frac{\mu_m \dot{\varepsilon}}{\Delta\rho g h_0} = \frac{\mu_m U_0}{\Delta\rho g h_0 L_\mathrm{r}} \dot{\varepsilon}' = \mu'_\mathrm{m} \dot{\varepsilon}', \tag{48}$$

where $\dot{\varepsilon}' = \dot{\varepsilon}\tau_\mathrm{r}$ is the nondimensionalized strain rate computed from the imposed mantle flow (see below). In practice the parameter we vary in these cases is μ'_m.

4.2.1. Two-Dimensional Cartesian Flow

In 2-D Cartesian coordinates we define

$$v_\mathrm{x} = \int_0^x \dot{\varepsilon}(x')dx', \tag{49}$$

$$v_\mathrm{z} = -\dot{\varepsilon}(x)z. \tag{50}$$

For a given function $\dot{\varepsilon}(x)$ these relations satisfy the conservation of mass and horizontal momentum in the vicinity of a thin layer at the CMB. For the particular examples below we will use the simple flow pattern:

$$\dot{\varepsilon}(x) = -\pi \frac{U_0}{L_\mathrm{r}} \cos\left(\frac{\pi x}{L_\mathrm{r}}\right), \tag{51}$$

which yields $u_\mathrm{x} = -U_0 \sin(\pi X/L_\mathrm{r})$ with upwelling mantle flow at $x = 0$ and downwelling flow at $x = L_\mathrm{r}$.

4.2.2. Axisymmetric Flow

We also consider the behavior of the thin layer in axisymmetric coordinates. Using an axial radius s we define

$$v_\mathrm{s} = \frac{1}{s}\int_0^s s'\dot{\varepsilon}(s')ds', \tag{52}$$

$$v_\mathrm{z} = -\dot{\varepsilon}(s)z. \tag{53}$$

Again, for a given function $\dot{\varepsilon}(s)$ these relations satisfy the conservation of mass and horizontal momentum in the vicinity of a thin layer at the CMB. For the 2-D axisymmetric model examples below we use a similar flow to the 2-D Cartesian case,

$$\dot{\varepsilon}(s) = -4\frac{U_0}{L_\mathrm{r}}\left(2 - \frac{3s}{L_\mathrm{r}}\right). \tag{54}$$

This gives a horizontal velocity of $u_\mathrm{s} = -4U_0\bar{s}(1-\bar{s})$ (where $\bar{s} = s/L_\mathrm{r}$) with downwelling flow at $s = L_\mathrm{r}$ and upwelling flow at $s = 0$.

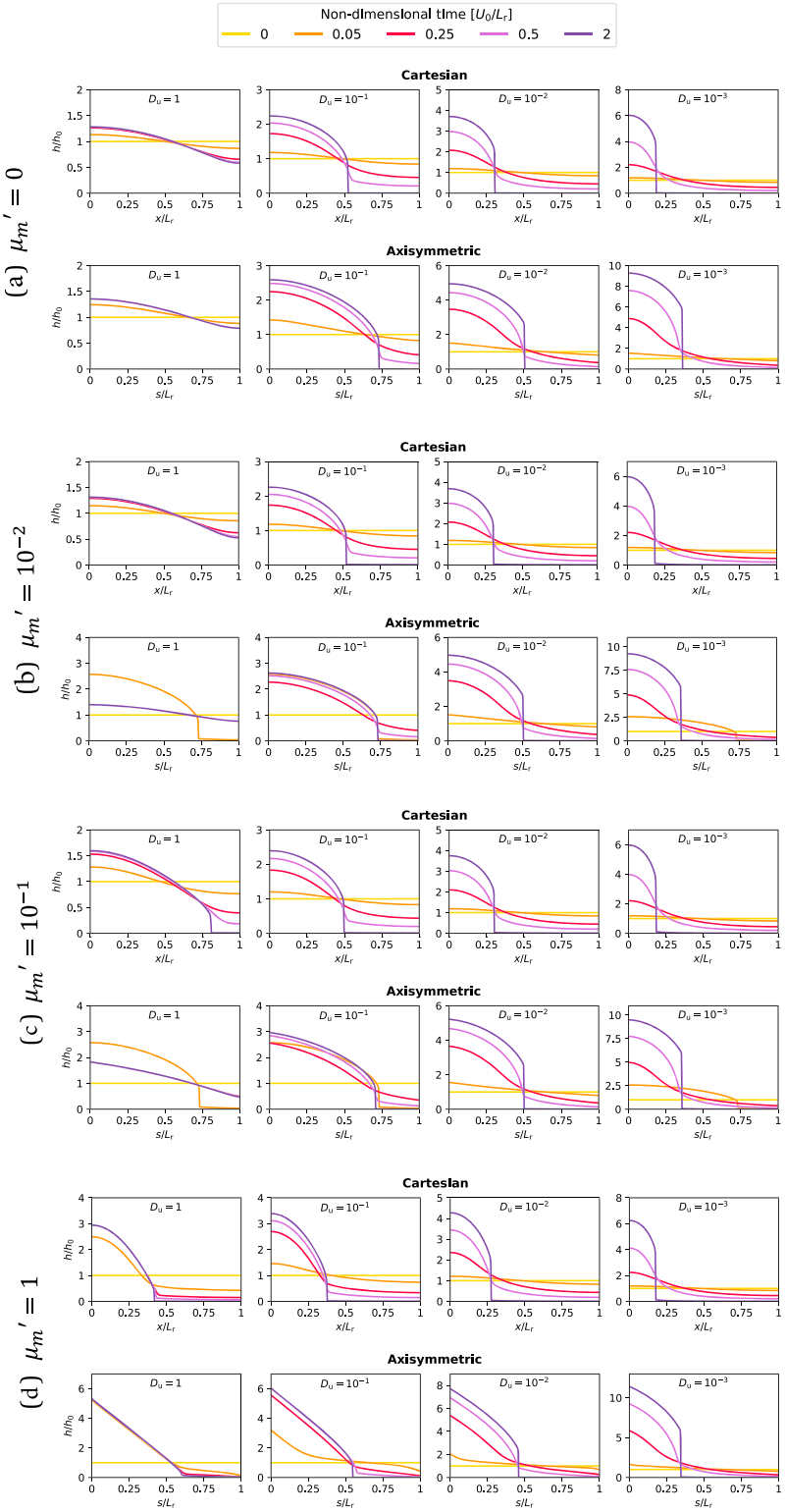

Figure 3. Evolution of the ultralow velocity zone layer for Cartesian and axisymmetric models when the influence of nondimensional diffusivity D_u and dynamic pressure μ'_m is varied (a–d). The height of the ultralow velocity zone layer is initially set to $h_0 = 1$ (yellow) and subsequently evolves until it reaches steady state (dark purple).

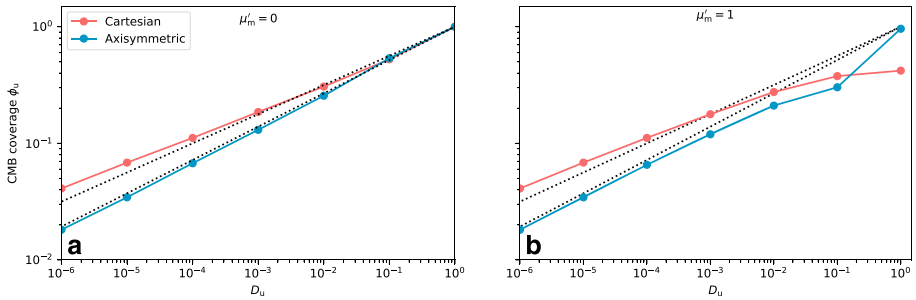

Figure 4. Ultralow velocity zone coverage at the core-mantle boundary (CMB) as a function of topography diffusivity D_u, for Cartesian and axisymmetric models (a) with and (b) without taking dynamic pressure effects into account. The dashed lines have slopes 1/4 and 2/7, as dictated by the power law in equation (60).

4.3. Time-Dependent Solutions

The time evolution of ULVZ layers, beginning from an initially flat state, is plotted in Figure 3. In almost every case, when $D_u \sim 1$ the layer remains continuous, with only modest undulations in the topography developing under the influence of the imposed mantle flow. In cases where $D_u \sim 10^{-1}$ or smaller, the ULVZ layer is swept toward the upwelling center and accumulates into a compact structure with sharp lateral boundaries bounded by regions with rapidly thinning ULVZ material (consistent with equation (32)). The time required for ULVZs to accumulate into isolated patches can be seen to be on the order of the residence time for mantle circulating through the CMB region L_r/U_0, and in all cases a steady state is attained by $\approx 2L_r/U_0$. This short equilibration time implies that dense ULVZ material at the CMB should not stably reside away from upwelling centers for geologically long periods of time, and its horizontal translation is controlled by lateral mantle flow.

The effect of dynamic pressure is to thicken the ULVZ profile at the axis of upwelling, giving the ULVZ an increasingly sloped profile as μ'_m and D_u increase. For reference, if we assume that $\mu_m = 10^{20}$ Pa s, $\dot{\epsilon}$=10^{-14} sec^{-1}, $\Delta\rho$ =500 kg/m^3, g =10 m/s^2, and $h_0 = 2$ km, then we would have $\mu'_m = 10^{-1}$. These parameters are uncertain, and therefore, the behavior of ULVZ at the CMB might occur in any of the forms shown in Figure 3. The total magnitude of the pressure effect in the governing equation is proportional to both D_u and μ'_m, and the influence of pressure is therefore greatest when both parameters become large. When $\mu'_m = 1$ the pressure effect can be great enough to create a distinct ULVZ island for $D_u = 1$ (Figure 3d) even though the layer would be continuous in the absence of pressure effects (Figure 3a). For modest values of μ'_m (Figures 3b and 3c), the solution for $D_u = 1$ begins with an island; however, it eventually evolves to a continuous layer at steady state.

4.4. Steady State Characteristics

For all parameters in which the layer is laterally discontinuous (see Figure 3), ULVZs exhibit sharp lateral edges and a relatively flat upper surface at steady state. Smaller values of diffusivity lead to more compact structures, while larger diffusivity leads to broader features. Note that the height is plotted relative to a reference height h_0 and that the integrated volume in the 2-D Cartesian case differs from the axisymmetric scenarios. In Figure 4 we plot the lateral (map area) coverage of the ULVZ layer as a function of D_u. Areal coverage is defined here as

$$\phi_u = \left(\frac{L_u}{L_r}\right)^N, \tag{55}$$

where L_u is the horizontal width of the ULVZ patch at steady state, $N = 1$ for the Cartesian case, and $N = 2$ for the axisymmetric case. Our results show a power law variation in the coverage of ULVZ patches ϕ_u as a function of D_u of the form $\phi_u \propto (D_u)^a$. The power law index a apparently assumes a different value depending on whether a 2-D Cartesian or axisymmetric geometry is considered. This relation breaks down when dynamic pressure is more important (right panel of Figure 4); however, it only has a significant influence at the largest values of D_u.

The relation $\phi_u \propto (D_u)^a$ can be understood by applying the steady state relations derived previously. First, we note that conservation of layer volume implies that

$$\phi_u \approx \frac{1}{h'_u}, \tag{56}$$

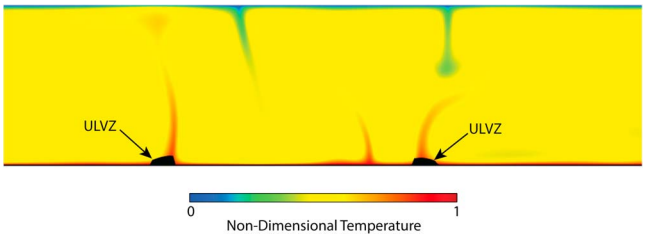

Figure 5. Snapshot of a solution for Rayleigh-Bénard convection showing the nondimensional temperature field and the ultralow velocity zone (ULVZ) layer profile (black features at the bottom). The ULVZ thickness is nondimensional, and they are vertically exaggerated here (relative to usual ULVZ thicknesses) in order to render them visible in the figure.

where h'_u is the steady state characteristic thickness of the ULVZ patches. We rewrite equation (46) as

$$\frac{h_u^3}{L_u} \sim \frac{3\mu\dot{\varepsilon}_u L_u}{\Delta\rho g}, \tag{57}$$

where $\dot{\varepsilon}_u$ is the horizontally convergent strain rate (velocity gradient) in the vicinity of the upwelling. We have substituted $\bar{U} \sim \dot{\varepsilon}_u L_u$ because the velocity is variable in the vicinity of the upwelling center, and hence, the layer (where it is thick) is subject to a different effective $\bar{U}$ depending on its width L_u. While this only accounts for the linear variations in velocity near the upwelling center, it is sufficient to predict the observed power law behavior.

The above cases are defined in terms of $D_{u,res}$; however, the power law value a can be derived by adopting another definition of D_u, namely,

$$D_{u,loc} = \frac{\Delta\rho g h_u^3}{3\mu\dot{\varepsilon}_u L_u^2}, \tag{58}$$

and at steady state we see from equation (57) that $D_{u,loc} \sim 1$. This result can be manipulated as follows:

$$1 \approx D_{u,loc} = D_{u,res}\left(\frac{U_0}{\dot{\varepsilon}_u L_r}\right)\left(\frac{L_r}{L_u}\right)^2 (h'_u)^3 = D_{u,res}\left(\frac{L_r}{L_u}\right)(h'_u)^3 = D_{u,res}\left(\frac{1}{\phi_u}\right)^{1/N+3}, \tag{59}$$

where we have substituted $U_0 = \dot{\varepsilon}_u L_u$ and used equations (55) and (56) to relate the expression to ϕ_u. Rearranging this result, we arrive at

$$\phi_u \approx \left(D_{u,res}\right)^{N/(1+3N)}. \tag{60}$$

As shown in Figure 4, the power law slopes of $a = 1/4$ and $a = 2/7$ (for Cartesian and axisymmetric geometries, respectively) predicted by this relation agree reasonably well with the numerical results when the effect dynamic pressure is not taken into account (see Figure 4a).

4.5. Implementation of the ULVZ Equation in Mantle Convection Models

The ULVZ equation can be solved for the evolution of a dense layer at the base of a convecting mantle and is straightforward to include in mantle convection codes. Here we show an example of solutions for the ULVZ equation in a Boussinesq, incompressible, isoviscous, infinite Prandtl number, bottom-heated convection model with free-slip upper and lower isothermal boundaries, and periodic side boundaries. The model was run using an Earth-like Rayleigh number of 5×10^6 (yielding time-dependent Rayleigh-Bénard convection). The numerical implementation is similar to the imposed mantle flow cases above; however, horizontal velocities at the lower boundary of the convection model are taken from the solution at each step for lateral advection of the ULVZ layer. The thermal convection model is run until characteristics reach a statistically steady state, and then a uniform thickness ULVZ layer is introduced, and then the solution for both the convection and the layer is resumed. For the example shown here, the influence of dynamic pressure is excluded since it only affects the shape of ULVZs. Time-dependent convection in these models causes hot plumes to migrate toward one another and merge, vacating a portion of the boundary layer and allowing new plumes to form away from preexisting plumes.

Figure 5 shows a snapshot of the evolution of the ULVZ layer for $D_u = 1$ and neglecting the influence of dynamic pressure (i.e., $\mu'_m = 0$). In this case D_u is defined using the mantle thermal diffusion time scale according to equation (41). The solution rapidly evolves to a state in which the ULVZ layer is aggregated into two distinct islands residing beneath upwelling thermal plumes. The ULVZ material follows these plume roots as they migrate laterally. The regions between these ULVZ islands do not contain any significant ULVZ material (i.e., $h' \approx 0$). Once the initial aggregation of ULVZ layer material beneath upwelling plumes has occurred, new plumes that form in the thermal boundary layer (away from preexisting plumes) have no source of material to aggregate a new ULVZ island. Thus, there are two populations of plumes: longer-lived plumes with ULVZ islands and younger plumes with no islands. We note that ULVZ structures beneath mobile plumes exhibit a sloped top, with the thicker portion at the leading edge and the thinner portion at the trailing edge. However, the inclusion of dynamic pressure could alter this effect owing to its contribution to a sloped ULVZ topography discussed in the previous section.

5. Constraints on ULVZ Physical Properties and Deep Mantle Flow

In a previous study Hier-Majumder and Revenaugh (2010) used the thin-layer approximation to arrive an an estimate for the viscosity of ULVZ, and our results offer additional support for the use of ULVZ structure to infer physical properties. However, it is important to emphasize that the quantity that can be constrained by this approach is actually D (or D_u), which is comprised of a combination of parameters that includes both the viscosity and density anomaly and is scaled by poorly constrained characteristics of mantle flow. In a previous development we derived a way of expressing D_u using a local definition that contains fewer uncertain terms and refers more specifically to the ULVZ structure, and this is most similar in nature to the approach utilized by Hier-Majumder and Revenaugh (2010).

In equation (59) we used $D_{u,loc} \sim 1$ to explain the power law relationship between areal coverage ϕ_u and D_u across a broad parameter range (in addition to differences in the 2-D Cartesian and axisymmetric scaling behavior). The relation $D_{u,loc} \sim 1$ may also be applied directly to seismic observations. For example, the geometry of an axisymmetric ULVZ rooted beneath Iceland is approximately constrained by the recent waveform analysis of Yuan and Romanowicz (2017). Using their values of $h_u \approx 15$ km and $L_u \approx 400$ km, along with $\Delta\rho/\rho \approx 0.1$ (Rost et al., 2005), and $g = 10$ m/s^2, we then have $\mu \approx 4 \times 10^4/\dot{\varepsilon}_u$. This implies that $\mu \sim 10^{18}$ Pa s if $\dot{\varepsilon}_u \sim 10^{-14}$ s^{-1}. This strain rate is plausible if this ULVZ is located at the root of a deep-seated upwelling Iceland plume, a context in which strain rates of 10^{-13} s^{-1} or larger might be permitted (e.g., upwelling plume flow velocities up to ~1 m/year fed by a ~1,000-km-wide root gives $\dot{\varepsilon}_u \sim 10^{-13}$ s^{-1}). Furthermore, if the ULVZ density anomaly is smaller than our assumed value of 10%, then the estimate for ULVZ viscosity must be smaller by a similar amount. Therefore, we consider $\mu \sim 10^{18}$ Pa s to be consistent with these seismic constraints, although we should be mindful of seismological uncertainties in h_u (which are amplified as h_u^3 in $D_{u,loc}$).

Another method for inferring D_u is to employ the power law relation with the areal coverage ϕ_u of ULVZ on the CMB. The ϕ_u constraint shows that the determination of D_u is not confounded by dynamic pressure variations for ULVZ coverages of order ~10% or less, which may be appropriate for the ULVZ coverage of the Earth's CMB. (Figure 4). For example, suppose that $\phi_u \approx 10\%$ at the Earth's CMB. Then, depending on whether the mantle flow occurs in a 2-D or axisymmetric context, the results in Figure 4 imply that D_u should be in the range $D_{u,res} = 10^{-4} - 10^{-3}$. If we use $\dot{\varepsilon}_u \sim 10^{-14}$ s^{-1}, $\mu \sim 10^{18}$ Pa s, and $\Delta\rho/\rho \approx 0.1$, consistent with the Iceland case above, then the ϕ_u ~10% constraint implies that $h_0^3/L_r^2 \sim 10^{-1}$ or less. Taking L_r ~1,000 km as an example then yields h_0 ~1 km. That is, the average global thickness of the ULVZ (if it were spread evenly over the CMB) is inferred to be of order 1 km, which is not dissimilar to some proposed estimates (Hernlund & McNamara, 2014).

6. Summary

The numerical examples described above illustrate that ULVZs comprised of a thin dense chemically distinct layer will quickly aggregate beneath upwelling centers on time scales of order τ_r (the residence time for mantle flow through the CMB region). Therefore, if ULVZs are indeed comprised of dense chemically distinct material, then we would expect them to be prefentially accumulated at the roots of deep-seated mantle plumes, or perhaps the edges of LLSVPs (Hernlund & Tackley, 2007; McNamara et al., 2010). This picture is consistent with a reported geographical correlation between hot spots that may be produced by deep-seated hot mantle plumes and the locations of ULVZs at the CMB (Williams et al., 1998). In our models, the edges of ULVZs are sharp, and the remainder of the CMB away from plume roots is bereft of ULVZ material, perhaps explaining why some areas of the CMB have no ULVZs present (e.g., Persh et al., 2001; Vidale & Benz, 1992). While this picture may be consistent with some observations, it is not clear that all reported ULVZs can easily be placed in the context of localized upwelling centers. If ULVZs can be identified in contexts that clearly contradict the predictions of the thin dense layer model, then those may require another causative explanation.

Our results in inferring the physical properties of ULVZs are in agreement with those obtained by Hier-Majumder and Revenaugh (2010) and broadly consistent with ULVZs that are ~10% more dense and having a viscosity of 10^{18} Pa s or smaller. Such a small viscosity and strong density contrast implies a significant difference in composition between ULVZs and overlying mantle, consistent with our treatment of a ULVZ as a thin compositionally distinct layer. Large viscosity contrasts might also be consistent with the presence of partial melt, which may be enabled by a ULVZ composition that endows the material with a

lower solidus temperature compared to the overlying mantle. However, when coupled with the large density constrast, partial melt must be coupled with (and perhaps induced by) the change in composition between ULVZs and overlying mantle. Recall that smaller density anomalies require proportionally smaller viscosities in order to satisfy the constraints derived above, causing difficulties for any argument that does not involve changes in composition.

The ULVZ equation represents a unique tool for exploring the dynamics of the CMB region. This time evolution equation can be added to any mantle convection code, allowing modelers to consider ULVZ dynamics in a variety of scenarios with relative ease and little computational expense. The results obtained by applying the ULVZ equation lend more confidence to the interpretation of these features as compositionally distinct, dense, and relatively low viscosity material. In the future this equation may also be useful for inclusion in statistical boundary models (e.g., Wu et al., 2011), interpreting seismological observations of ULVZ, and may facilitate studies that seek to combine dynamical modeling and waveform analysis (e.g., van den Berg et al., 2010).

Acknowledgments
This manuscript benefited from discussions and reviews by Saswata Hier-Majumder and David A. Yuen. I. B. acknowledges financial support from a scholarship by the Japanese Ministry of Education, Culture, Sports, Science and Technology (MEXT). All model input parameters are given in section 4 and Figures 3 and 4.

References

Cottaar, S., & Romanowicz, B. (2012). An unusually large ULVZ at the base of the mantle near Hawaii. *Earth and Planetary Science Letters*, *355–356*, 213–222.

Garnero, E., & Helmberger, D. (1996). Seismic detection of a thin laterally varying boundary layer at the base of the mantle beneath the central-Pacific. *Geophysical Research Letters*, *23*(9), 977–980.

Garnero, E. J., & McNamara, A. K. (2008). Structure and dynamics of Earth's lower mantle. *Science*, *320*(5876), 626–628.

Garnero, E. J., McNamara, A. K., & Shim, S.-H. (2016). Continent-sized anomalous zones with low seismic velocity at the base of Earth's mantle. *Nature Geoscience*, *9*, 481–489. https://doi.org/10.1038/ngeo2733

Helmberger, D. V., Wen, L., & Ding, X. (1998). Seismic evidence that the source of the Iceland hotspot lies at the core-mantle boundary. *Nature*, *396*, 251–255.

Hernlund, J. W. (2010). On the interaction of the geotherm with a post-perovskite phase transition in the deep mantle. *Physics of the Earth and Planetary Interiors*, *180*(3), 222–234.

Hernlund, J. W., & Jellinek, M. (2010). Dynamics and structure of a stirred partially molten ultralow-velocity zone. *Earth and Planetary Science Letters*, *296*, 1–8.

Hernlund, J. W., & McNamara, A. K. (2014). Dynamics of the core mantle boundary region, (2nd edition). In G. Schubert & D. Bercovici (Eds.), *Treatise on geophysics* (pp. 461–519). Oxford: Elsevier.

Hernlund, J. W., & Tackley, P. J. (2007). Some dynamical consequences of partial melting in Earth's deep mantle. *Physics of the Earth and Planetary Interiors*, *162*(1), 149–163.

Hier-Majumder, S., & Drombosky, T. W. (2016). Coupled flow and anisotropy in the ultralow velocity zones. *Earth and Planetary Science Letters*, *450*, 274–282.

Hier-Majumder, S., & Revenaugh, J. (2010). Relationship between the viscosity and topography of the ultralow-velocity zone near the core-mantle boundary. *Earth and Planetary Science Letters*, *299*(3), 382–386.

Jellinek, A. M., & Manga, M. (2002). The influence of a chemical boundary layer on the fixity, spacing, and lifetime of mantle plumes. *Nature*, *418*, 760–763.

Jellinek, A. M., & Manga, M. (2004). Links between long-lived hot spots, mantle plumes, D$''$, and plate tectonics. *Reviews of Geophysics*, *42*, RG3002. https://doi.org/10.1029/2003RG000144

Jensen, K. J., Thorne, M. S., & Rost, S. (2013). SPdKS analysis of ultralow-velocity zones beneath the western Pacific. *Geophysical Research Letters*, *40*, 4574–4578. https://doi.org/10.1002/grl.50877

Kanda, RaviV. S., & Stevenson, D. J. (2006). Suction mechanism for iron entrainment into the lower mantle. *Geophysical Research Letters*, *33*, L02310. https://doi.org/10.1029/2005GL025009

Karato, S.-I. (2014). Does partial melting explain geophysical anomalies? *Physics of the Earth and Planetary Interiors*, *228*, 300–306.

Labrosse, S., Hernlund, J. W., & Coltice, N. (2007). A crystallizing dense magma ocean at the base of the Earth's mantle. *Nature*, *450*, 866–869.

Labrosse, S., Hernlund, J. W., & Hirose, K. (2015). Fractional melting and freezing in the deep mantle and implications for the formation of a basal magma ocean. In J. Badro & M. Walter (Eds.), *The early Earth: Accretion and differentiation* (Vol. 212, pp. 123–142). Hoboken, NJ: American Geophysical Union.

Laneuville, J. H., Labrosse, S., & Guttenberg, N. (2018). Crystallization of a compositionally stratified basal magma ocean. *Physics of the Earth and Planetary Interiors*, *276*, 86–92.

Li, M., McNamara, A. K., Garnero, E. J., & Yu, S. (2017). Compositionally-distinct ultra-low velocity zones on Earth's core-mantle boundary. *Nature Communications*, *8*(1), 177.

McNamara, A. K., Garnero, E. J., & Rost, S. (2010). Tracking deep mantle reservoirs with ultra-low velocity zones. *Earth and Planetary Sciences Letters*, *299*(1-2), 1–9.

Nomura, R., Ozawa, H., Tateno, S., Hirose, K., Hernlund, J., Muto, S., et al. (2011). Spin crossover and iron-rich silicate melt in the Earth's deep mantle. *Nature*, *473*(7346), 199–202.

Ohtani, E., & Maeda, M. (2001). Density of basaltic melt at high pressure and stability of the melt at the base of the lower mantle. *Earth and Planetary Science Letters*, *193*, 69–75.

Persh, S. E., Vidale, J. E., & Earle, P. S. (2001). Absence of short-period ULVZ precursors to PcP and ScP from two regions of the CMB. *Geophysical Research Letters*, *28*, 859–862.

Petford, N., Rushmer, T., & Yuen, D. A. (2013). Deformation-induced mechanical instabilities at the core-mantle boundary. In K. Hirose (Ed.), *Post-perovskite: The last mantle phase transition* (Vol. 174, pp. 271–287). American Geophysical Union (AGU).

Reynolds, O. (1886). I. On the theory of lubrication and its application to Mr. Beauchamp Tower's experiments, including an experimental determination of the viscosity of olive oil. *Proceedings of the Royal Society of London*, *40*(242-245), 191–203.

Rost, S., Garnero, E., Williams, Q., & Manga, M. (2005). Seismic constraints on a possible plume root at the core-mantle boundary. *Nature*, *435*, 666–9.

Thorne, M. S., Garnero, E. J., Jahnke, G., Igel, H., & McNamara, A. K. (2013). Mega ultra low velocity zone and mantle flow. *Earth and Planetary Science Letters*, *364*, 59–67.

van den Berg, A. P., De Hoop, M. V., Yuen, D. A., Duchkov, A., van der Hilst, R. D., & Jacobs, M. H. G. (2010). Geodynamical modeling and multiscale seismic expression of thermo-chemical heterogeneity and phase transitions in the lowermost mantle. *Physics of the Earth and Planetary Interiors*, *180*(3), 244–257.

Vidale, J. E., & Benz, H. M. (1992). A sharp and flat section of the core-mantle boundary. *Nature*, *359*, 627–629.

Wicks, J. K., Jackson, J. M., & Sturhahn, W. (2010). Very low sound velocities in iron-rich (Mg,Fe)O: Implications for the coremantle boundary region. *Geophysical Research Letters*, *37*, L15304. https://doi.org/10.1029/2010GL043689

Williams, Q., & Garnero, E. J. (1996). Seismic evidence for partial melt at the base of Earth's mantle. *Science*, *273*(5281), 1528–1530.

Williams, Q., Revenaugh, J. S., & Garnero, E. J. (1998). A correlation between ultra-low basal velocities in the mantle and hot spots. *Science*, *281*, 546–549.

Wu, B., Driscoll, P., & Olson, P. (2011). A statistical boundary layer model for the mantle D'' region. *Journal of Geophysical Research*, *116*, B12112. https://doi.org/10.1029/2011JB008511

Yuan, K., & Romanowicz, B. (2017). Seismic evidence for partial melting at the root of major hot spot plumes. *Science*, *357*, 393–397.